SCIENCE CHINA
Technological Sciences

April 2012 Vol.55 No.4: 990–996
doi: 10.1007/s11431-012-4752-6

Optimization design and analysis of Si-^{63}Ni betavoltaic battery

TANG XiaoBin, DING Ding, LIU YunPeng & CHEN Da*

Department of Nuclear Science and Engineering, Nanjing University of Aeronautics and Astronautics, Nanjing 210016, China

Received November 5, 2011; accepted December 26, 2011; published online February 7, 2012

Among the various micro-powers being investigated, betavoltaic batteries are very attractive for numerous applications because of their advantages of high energy density, long life, strong anti-interference, and so on. Based on the basic principle of the betavoltaic effect, the current paper adopted the Monte Carlo N-Particle code to simulate the transport processes of β particles in semiconductor materials and to establish the calculation formulas for nuclear radiation-generated current, open circuit voltage, and so on. By discussing the effect of minority carrier diffusion length, doping concentration, and junction depth on the property of batteries, the present work concluded that the best parameters for batteries are the use of silicon and the radioisotope Ni-63, i.e., Ni-63 with a mass thickness of 1 mg/cm^2, N_a=1×10^{19} cm^{-3}, N_d=3.16×10^{16} cm^{-3}, junction area of 1 cm^2, junction depth of 0.3 μm, and so on. Under these parameters the short-circuit current, open circuit voltage, output power, and conversion efficiency are 573.3 nA, 0.253 V, 99.85 nW, and 4.94%, respectively. Such parameters are valuable for micro-power fields, such as micro-electromechanical systems and pacemakers, among others.

betavoltaic, semiconductor material, radioisotope battery

Citation: Tang X B, Ding D, Liu Y P, et al. Optimization design and analysis of Si-^{63}Ni betavoltaic battery. Sci China Tech Sci, 2012, 55: 990–996, doi: 10.1007/s11431-012-4752-6

Compared with traditional micro-powers, radioisotope batteries that use the energy from the decay of radioisotopes can function without refueling and still meet the requirements of micro-electromechanical systems (MEMS) because of their simple structure, long life, and ease of integration. Among this type of batteries, betavoltaic batteries are very effective in solving the energy supply issue of MEMS because of their advantages of high energy density, small volume, strong anti-interference, high energy conversion efficiency [1, 2] and so on. However, research on betavoltaic batteries is still in its infancy. Betavoltaic batteries are made based on a silicon and PN junction, as well as have very low output power and energy conversion efficiency. Sun et al. of the Northwestern Polytechnical University developed ^{63}Ni-Si batteries with 0.79 nW/mm^2 output power and 0.767% conversion efficiency [3]. The Guo et al. of Xiamen University developed ^{147}Pm-Si batteries with 4.89 nW/mm^2 output power and 1.75% conversion efficiency [4]. Deus developed ^{3}H-Si (amorphous silicon) batteries with 1.36 nW/mm^2 output power and 1.2% conversion efficiency [5].

The current paper establishes a theoretical calculation model of planar betavoltaic batteries using the semiconductor material, Si and radioisotope, ^{63}Ni. Based on the basic principles of the betavoltaic effect, the Monte Carlo N-Particle (MCNP) code was used to simulate the transport processes of β particles in semiconductor materials and to establish the calculation formulas for nuclear radiation-generated current, open circuit voltage, and so on. The best parameters for batteries were determined by investigating the effects of minority carrier diffusion length, doping concentration, and junction depth on the property of batteries.

*Corresponding author (email: dachen@nuaa.edu.cn)

© Science China Press and Springer-Verlag Berlin Heidelberg 2012

© 1994-2012 China Academic Journal Electronic Publishing House. All rights reserved. http://www.cnki.net

1 Theoretical calculation model

1.1 Structure and theory of betavoltaic batteries

Figure 1 shows that a conventional single planar betavoltaic battery primarily comprises a radioisotope, a semiconductor, and electrode materials. The emission of energetic β particles from the radioisotope irradiate the semiconductor junction, thus resulting in the generation of electron hole pairs (EHPs) through ionization and excitation. The EHPs generated within the depletion region, and one minority carrier diffusion length of the depletion region is swept across the junction by the depletion electric field into the external load to produce electrical power.

1.2 Calculation of nuclear radiation-generated current

In previous studies, the calculation of nuclear radiation-generated current was primarily based on the theoretical model of Schockley on the semiconductor PN junction. Under certain assumptions, the current density and carrier continuity equations were established. The equations were then solved, and the current was obtained with certain boundary conditions. However, this kind of analytical calculation process is too complex, with the assumption that simplified conditions are often used to facilitate the solution at the expense of accuracy [6, 7]. The Monte Carlo method is one of the most accurate approaches for simulating the transport process of radioactive particles in materials. Therefore, the Monte Carlo simulation computer program MCNP is used to calculate the energy deposition of β particles by simulating the transport process of such particles after being emitted from radioisotope in semiconductor materials. The nuclear radiation-generated current is then obtained. Compared with the analytical solution presented above, this kind of solution significantly simplifies the calculation process, and the accuracy of the calculation results is guaranteed because of the high-precision MCNP calculations [8, 9].

Theoretically, the generation rate of EHPs in a unit thickness semiconductor can be obtained by

$$G = A \cdot E / \varepsilon, \tag{1}$$

where A is the activity of radioisotope, E is the energy deposition of a single β particle in the semiconductor calculated by MCNP, and ε is the average energy needed to generate an electron hole pair. For Si, ε is 3.64 eV.

Electron-hole collection probability is determined to be 100% for carriers generated inside the depletion region, whereas for carriers generated outside the depletion region, this probability can be obtained using the following equation [10, 11]:

$$CE = 1 - \tanh \frac{d}{L}, \tag{2}$$

where d is the distance from the depletion region, L is the minority carrier diffusion length, and tanh is the hyperbolic tangent function.

The nuclear radiation-generated current can then be calculated by

$$I_R = \int_0^H CE(x) \cdot q \cdot G(x) \mathrm{d}x = \frac{qA}{\varepsilon} \int_0^H CE(x) \cdot E(x) \mathrm{d}x = \frac{qA}{\varepsilon} \sum_{n=1}^{k} CE(n) \cdot E(n), \tag{3}$$

where H is the thickness of the semiconductor, $CE(x)$ is the collection probability of electro hole pairs, q is the electron charge, $E(x)$ is the energy deposition, $E(n)$ is the energy deposition of the Nth layer semiconductor calculated by MCNP, and k is the number of total layers in the semiconductor during MCNP calculation.

1.3 Calculation of electrical properties

From its equivalent circuit model, the short-circuit current I_{SC}, the open-circuit voltage V_{OC}, and the maximum output power P_m can be derived as [7]

$$I_{SC} = I_R, \tag{4}$$

$$V_{OC} = \frac{kT}{q} \ln\left(\frac{I_R}{I_0} + 1\right), \tag{5}$$

$$P_m = FF \cdot V_{OC} \cdot I_{SC}, \tag{6}$$

where k is Boltzmann's constant, T is the absolute temperature, I_0 is the leakage current of PN junction, and FF is the filling factor.

The FF can be calculated by [8]

$$FF = \frac{v_{OC} - \ln(v_{OC} + 0.72)}{v_{OC} + 1}, \tag{7}$$

where v_{OC} is the normalized open-circuit voltage and

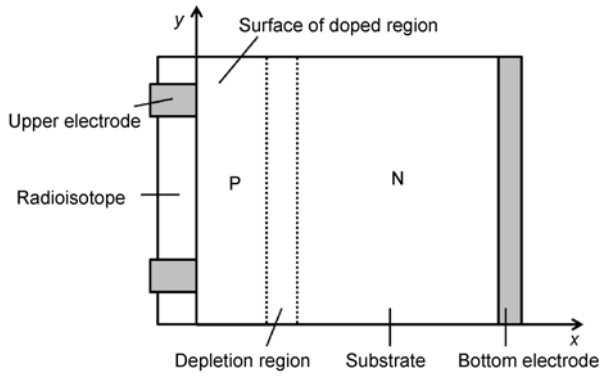

Figure 1 Schematic diagram of planar betavoltaic batteries.

© 1994-2012 China Academic Journal Electronic Publishing House. All rights reserved. http://www.cnki.net

$v_{OC} = \dfrac{qV_{OC}}{kT}$.

The conversion efficiency can be calculated by

$$\eta = \frac{P_m}{P_{in}} = \frac{FF \cdot V_{OC} \cdot I_{SC}}{A\overline{E}q}, \tag{8}$$

where P_m is the maximum output power, P_{in} is the incident power of β particles, A is the activity of radioisotope, $\overline{E}$ is the average energy of incident β particles, and q refers to the electron charge.

2 Optimization and analysis

Single crystal silicon, the most mature semiconductor studied to date, has already been widely used in betavoltaic batteries because of its high temperature resistance, anti-radiation properties, and so on. The selection of the radioisotope is based on safety, reliability, half-life, damage to the semiconductor materials, and other factors. The energy of β particles emitted from ^{63}Ni is 0 eV to 66.7 keV, and the average kinetic energy is 17.1 keV. The radioactive particles with the 66.7 keV maximum kinetic energy cannot penetrate through the skin of a person because its value is far lower than the threshold value, that is, 200 keV to 250 keV. This threshold value may result in unrecoverable damage to the silicon lattice. Therefore, single crystal silicon and ^{63}Ni were selected as the subjects in the current paper.

2.1 Self-absorption effect of the radioisotope

β particles emitted from the decay of radioisotopes will lose energy during transportation. Thus, the surface source activity and surface-emitting power are weakened. That is, a self-absorption phenomenon emerges. Figure 2 shows the relationship between the surface source (single surface) activity (A_S) of ^{63}Ni radioisotope with different abundances calculated via the MCNP code and the mass thickness (T_m). The surface source activity is shown to increase with increasing mass thickness. However, when the mass thickness is approximately 5.2 mg/cm^2, the surface source activity is saturated. The surface activity is approximately 80% of the saturated surface source activity when the mass thickness is 1 mg/cm^2. Therefore, the ^{63}Ni radioisotope with 1 mg/cm^2 mass thickness is selected for the maximization of source utilization.

2.2 Energy deposition of β particles in semiconductor

The energy deposition distribution and accumulated energy deposition of β particles emitted by ^{63}Ni with a mass thickness of 1 mg/cm^2 along the direction of silicon semiconductor thickness are calculated using MCNP, as shown in Figure 3. The graph shows that the energy of β particles is

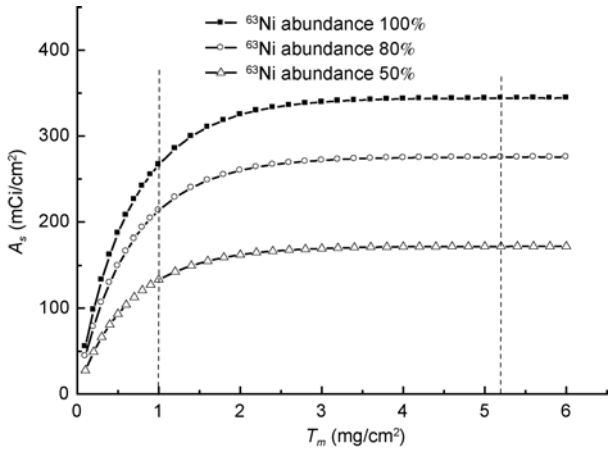

Figure 2 Plot of surface activity as a function of mass thickness for ^{63}Ni.

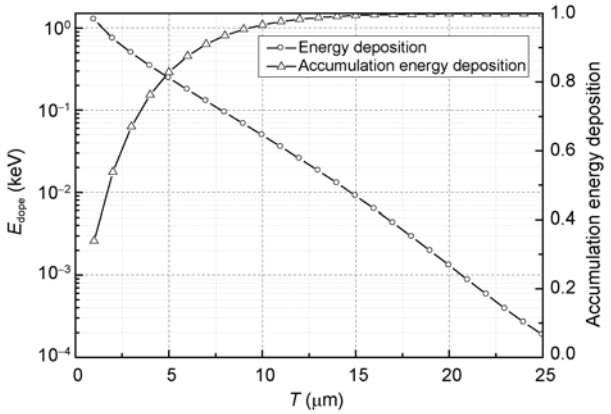

Figure 3 Energy depositions in Si for ^{63}Ni.

primarily deposited on the surface layer of the semiconductor and that the deposited energy is distributed along the direction of thickness in a form of approximate exponential. The proportion of accumulated deposition energy into the total deposited energy will be 80% when the thickness of semiconductor is approximately 5 μm, and when the thickness is approximately 20 μm, the proportion reaches 99.9%.

2.3 Minority carrier diffusion length

The minority carrier diffusion length L is the average distance traveled by a minority carrier in a semiconductor. Eq. (2) shows that the minority carrier diffusion length is the factor directly affecting the collection efficiency of the carrier. Thus, a longer minority carrier diffusion makes it easier for EHPs generated outside the depletion region to diffuse to the depletion region, thus contributing significantly to the nuclear radiation-generated current. The battery performance can then be increased accordingly.

The minority carrier diffusion length can be calculated by

© 1994-2012 China Academic Journal Electronic Publishing House. All rights reserved. http://www.cnki.net

$$L = \sqrt{D\tau} = \sqrt{\frac{kT}{q}\mu\tau}, \tag{9}$$

where D refers to the diffusion coefficient, τ refers to the minority carrier life, and μ refers to the minority carrier mobility.

For Si semiconductor, based on the minority carrier mobility and the empirical formula of minority carrier life, the minority carrier diffusion length of P-type region and N-type region can be respectively represented by [12]

$$L_n = \sqrt{\frac{kT}{q}\left[232 + \frac{1180}{1+\left(\frac{N_a}{8\times10^{16}}\right)^{0.9}}\right]\cdot\frac{1}{3.45\times10^{-12}N_a + 9.5\times10^{-32}N_a^2}}, \tag{10}$$

$$L_p = \sqrt{\frac{kT}{q}\left[130 + \frac{370}{1+\left(\frac{N_d}{8\times10^{17}}\right)^{1.25}}\right]\cdot\frac{1}{7.8\times10^{-13}N_d + 1.8\times10^{-31}N_d^2}}, \tag{11}$$

where L_n and N_a respectively refer to the minority carrier (electron) diffusion length and doping concentration of P-type region; L_p and N_d respectively refer to the minority carrier (hole) diffusion length and doping concentration of N-type region, where the unit of diffusion length is μm and that of doping concentration is cm^{-3}.

From empirical equations (10) and (11), the relationship between the minority carrier diffusion length and doping concentration in Si semiconductor under the normal temperature (300 K) can be obtained, as shown in Figure 4. Thus, the doping concentration is the primary factor affecting the minority carrier diffusion length. With the increase in doping concentration, the minority carrier length rapidly reduces to no more than 1 μm at 10^{20} cm^{-3} from 1000 μm at 10^{15} cm^{-3} of doping concentration.

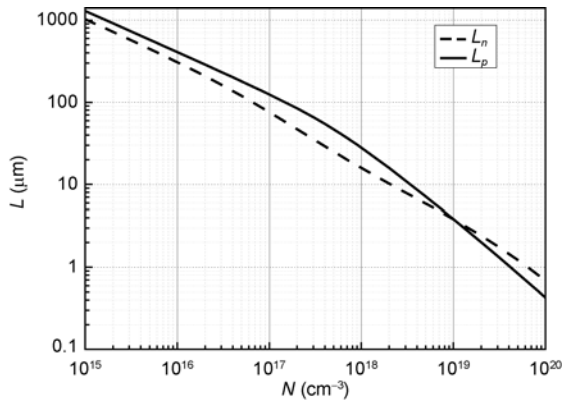

Figure 4 Plot of minority carrier diffusion length as a function of doping concentration.

2.4 Width of the depletion region

Eq. (2) indicates that the EHPs generated outside the depletion region are associated with the distance between the depletion region (d) and the minority carrier diffusion length. Regions closer to the depletion region generally have a higher collection efficiency. The EPHs generated inside the depletion region are completely collected. A wider width of the depletion region yields more contributions to the short-circuit current. Therefore, the width of the depletion region is an important parameter affecting the battery performance.

The width of the depletion region, W, is given by [12]

$$W = \sqrt{V_D\left(\frac{2\varepsilon_r\varepsilon_0}{q}\right)\left(\frac{N_a+N_d}{N_aN_d}\right)}, \tag{12}$$

$$V_D = \frac{kT}{q}\left(\ln\frac{N_aN_d}{n_i^2}\right), \tag{13}$$

where V_D is the built-in potential difference; ε_r is the dielectric constant; ε_0 is the vacuum dielectric constant; N_a and N_d are doping concentrations of P-type and N-type regions, respectively; and n_i is the intrinsic carrier concentration.

From eq. (12), the graph of the relationship between the width of the depletion region and the doping concentration of each region can be obtained, as shown in Figure 5. The width of depletion region varies significantly with the doping concentration. As for the unilateral abrupt junction, the width of the depletion region is primarily associated with the low doping concentration. A lower doping concentration results in a wider depletion region.

2.5 Leakage current of the PN junction

As indicated by eq. (5), the leakage current of the PN junction is the parameter directly affecting the open-circuit voltage of the battery. The open-circuit voltage increases with the decreasing leakage current of the PN junction. Figure 6 shows the relationship between the open-circuit voltage V_{OC} and I_R/I_0 (the ratio of nuclear radiation-generated current into the leakage current of PN junction) under normal temperature (300 K).

The value of I_R/I_0 should be greater than 1000 to obtain a high open-circuit voltage. For a solar battery, the nA-μA leakage current of the PN junction imposes small effects on the solar battery because the magnitude order of the photovoltaic current is mA to 100 mA. However, in case of the betavoltaic battery for which pA-nA is of the magnitude order of nuclear radiation-generated current, nA-μA which

© 1994-2012 China Academic Journal Electronic Publishing House. All rights reserved. http://www.cnki.net

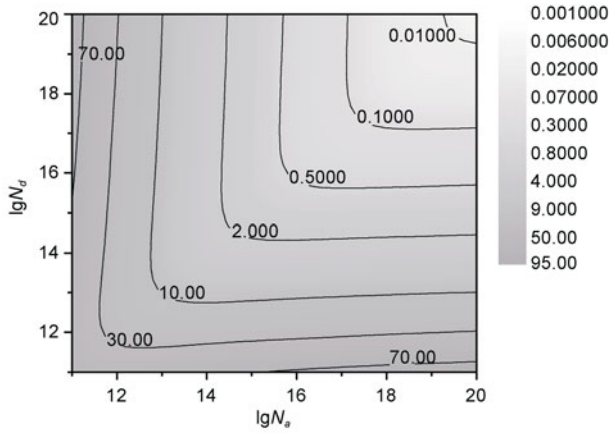

Figure 5 Plot of depletion width as a function of doping concentration.

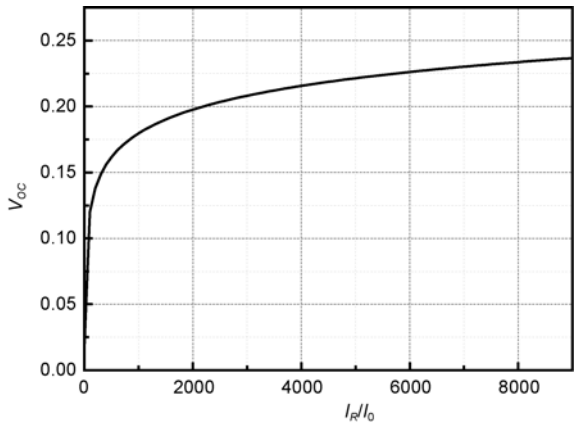

Figure 6 Plot of open circuit voltage as a function of the ratio of nuclear radiation-generated current to the leakage current.

is of the magnitude order of leakage current is so large that the battery can barely generate electric energy.

The leakage current of the PN junction can be calculated using [12]

$$I_0 = Sqn_i^2\left(\frac{D_p}{L_pN_d}+\frac{D_n}{L_nN_a}\right), \tag{14}$$

where S is the junction area, n_i is the intrinsic carrier concentration, $D_{p\,(n)}$ is the minority carrier diffusion efficiency, $L_{p\,(n)}$ is the minority carrier diffusion length, and $N_{d\,(a)}$ is the doping concentration.

The primary parameters affecting the leakage current of the PN junction are temperature, junction area, and doping concentration. Figure 7 shows the relationship between the leakage current of the Si PN junction and the doping concentration under the conditions of 300 K and 1 cm^2 junction area. The leakage current of the PN junction increases with the reduction of the doping concentration in the P-type and N-type regions. The effects of the doping concentration of the P-type region N_a on the leakage current of the PN junction is more significant than those of the

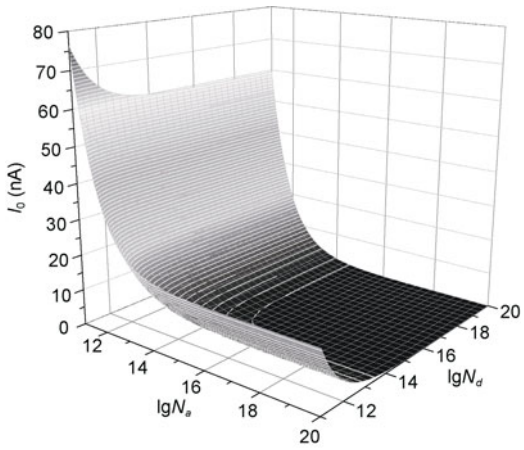

Figure 7 Plot of leakage current as a function of doping concentration.

N-type region N_d, especially in case of low doping concentration.

2.6 Doping concentration

By the analysis above, the doping concentration is shown to determine the minority carrier diffusion length of the PN junction, the depletion region width, and the leakage current. Low doping concentration will result in a longer minority carrier diffusion length and a wider depletion region width. The condition will be favorable for the collection of EHPs, and the short-circuit current of the battery will increase accordingly. On the other hand, low doping concentration will result in an increase in the leakage current and a reduction in the open-circuit voltage. Therefore, the optimal design of the battery has to consider these two factors, and the appropriate doping concentration must be selected to maximize the output power.

The computation of maximum output power involves numerous parameters, such as temperature, radioisotope activity, junction area and depth, and so on. Directly analyzing the effects of the doping concentration on output power is not easy. Therefore, a numerical analysis and simulation of short-circuit current, open-circuit voltage, and the maximum output power of the battery were conducted using the mathematical analysis software MATLAB.

Figure 8 shows the relationship between the maximum output power and doping concentration under the condition of 300 K, 1 mg/cm^2 mass thickness of ^{63}Ni radioisotope, 100 mCi of the source activity (the single surface source activity is about 19.6 mCi), and 0.5 μm junction depth. The doping concentration unit is cm^{-3}, and the power unit is nW. Under the aforementioned parameter conditions, heavy doping (the doping concentration is at the magnitude order of 10^{18} cm^{-3} to 10^{19} cm^{-3}) in the surface doping region (that is, the P-type region, where the doping concentration is N_a) and light doping (the doping concentration is at the magnitude orders of 10^{16} cm^{-3} to 10^{17} cm^{-3}) in the substrate region

© 1994-2012 China Academic Journal Electronic Publishing House. All rights reserved. http://www.cnki.net

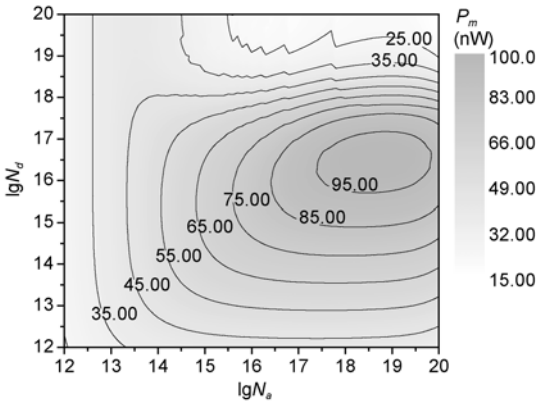

Figure 8 Maximum output power vs. doping concentration.

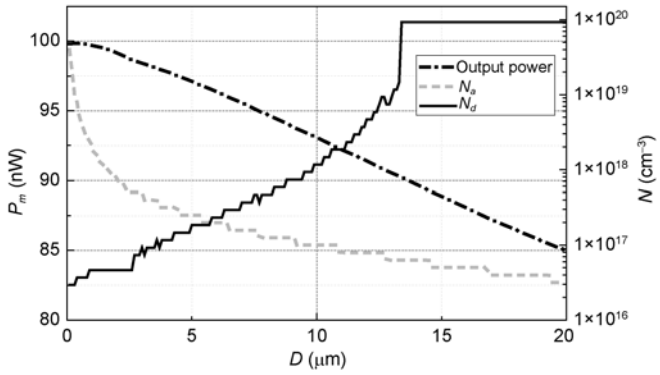

Figure 9 Maximum output power and optimal doping concentrations vs. junction depth.

(that is, the N-type region, where the doping concentration is N_d) can yield the highest output power.

2.7 Junction depth

Table 1 shows the maximum output power and other corresponding parameter values of the battery under different junction depths under the condition of 300 K, 1 mg/cm^2 mass thickness of ^{63}Ni radioisotope, 100 mCi of the source activity (the single surface source activity is about 19.6 mCi), 1 cm^2 junction area, which was calculated by Matlab. It's shown that short-circuit current and conversion efficiency reach the highest when the junction depth is 0.3 μm.

In addition, the changes in junction depth between 0 μm and 20 μm, the battery's maximum output power, and the corresponding optimal doping concentration were also given in the current paper, as shown in Figure 9. The maximum output power can be observed to basically decrease with the increasing depth, whereas the optimal doping concentrations of the P-type and N-type regions increase according to the changes in the junction depth. When the junction depth is relatively low, taking heavy doping in the P-type region and light doping in the N-type region is appropriate.

2.8 Internal resistance of the battery and width of substrate

The internal resistance of a battery includes both shunt and series resistances. The open-circuit voltage and short-circuit current can be increased by enhancing shunt resistance and reducing series resistance. Selecting a good single crystal substrate is necessary to increase the shunt resistance. Moreover, less lattice defects and surface contamination are required, among others. This condition also enables the reduction of the low leakage current of the PN junction. The series resistance primarily includes the bulk resistance of the batter, the resistance of the metal electrode, as well as the contact resistance of the metal electrode and semiconductor.

The bulk resistance of battery is defined as

$$R = \frac{\rho H}{S}, \tag{15}$$

where ρ is the bulk resistivity, H is the thickness of semiconductor, and S is the unction area. The bulk resistivity ρ primarily depends on the doping concentration of the base region. A higher doping concentration of the base region results in lower bulk resistivity. A greater thickness of the

Table 1 Maximum output power and other corresponding parameter values of the battery under different junction depths

Junction depth (μm)	Maximum output power (nW)	Doping concentration of P-type region (cm^{-3})	Doping concentration of N-type region (cm^{-3})	Short-circuit current (nA)	Open-circuit voltage (V)	Conversion efficiency (%)
0.1	99.829	3.98×10^{19}	3.16×10^{16}	571.100	0.253	4.939
0.2	99.851	2.00×10^{19}	3.16×10^{16}	572.035	0.253	4.940
0.3	99.847	1.00×10^{19}	3.16×10^{16}	573.347	0.253	4.940
0.4	99.851	7.94×10^{18}	3.98×10^{16}	567.057	0.255	4.940
0.5	99.842	5.01×10^{18}	3.98×10^{16}	568.624	0.254	4.940
0.6	99.826	3.98×10^{18}	3.98×10^{16}	569.543	0.254	4.939
0.7	99.798	3.16×10^{18}	3.98×10^{16}	570.553	0.254	4.938
0.8	99.760	2.51×10^{18}	3.98×10^{16}	571.684	0.253	4.936
0.9	99.718	2.51×10^{18}	5.01×10^{16}	565.196	0.255	4.934

© 1994-2012 China Academic Journal Electronic Publishing House. All rights reserved. http://www.cnki.net

semiconductor results in higher bulk resistivity. Therefore, controlling the thickness of the base region and then determining the width of the surface doping and depletion regions are necessary. That is, the thickness of the base region should be smaller than the sum of minority carrier diffusion length of the base region and the width of the depletion region.

The contact resistance of the metal electrode and semiconductor is primarily related to the work function of these materials. As for the surface heavy doping region of boron doping, the doping concentration generally ranges from 10^{19} cm^{-3} to 10^{20} cm^{-3} to realize good ohmic contact with the electrode metal. Therefore, by referring to Table 1 and the aforementioned analysis, the optimum junction depth is to be 0.3 μm, the doping concentration of the surface heavy doping region (P-type region) is 1×10^{19} cm^{-3}, and the base region depth (N-type region) is 3.16×10^{16} cm^{-3}. Under this condition, the minority carrier diffusion length of the substrate is approximately 164 μm, whereas when considering the restrictions of the technology, such as silicon slice polishing reduction, the total thickness of the semiconductor shall be approximately 160 μm.

3 Conclusion

The current paper established a theoretical calculation model of planar betavoltaic batteries using the semiconductor material, Si, and radioisotope ^{63}Ni. Based on the fundamental principle of the betavoltaic effect, the influencing mechanism of each factor on the performance parameters of the battery was analyzed through the simulation of the transport process of β particles in the semiconductor material using the Monte Carlo simulation program MCNP. The optimized design parameters of a planar betavoltaic battery were then determined. That is, the mass thickness of radioisotope ^{63}Ni is 1 mg/cm^2, the doping concentration of P-type region is 1×10^{19} cm^{-3} and that of N-type region is 3.16×10^{16} cm^{-3}, the junction area is 1 cm^2, the junction depth is 0.3 μm, and the total thickness of the battery does not exceed 160 μm. In this case, provided that the radioisotope activity is 100 mCi, the obtained maximum short-circuit current, open-circuit voltage, output power, and conversion efficiency can be obtained as 573.3 nA, 0.253 V, 99.85 nW, and 4.94%, respectively. The result of the current paper can provide a significant theoretical reference for the fabrication of Si-^{63}Ni betavoltaic batteries.

This work was supported by the China Postdoctoral Science Foundation Funded Project (Grant No. 20100481140) and the Nanjing University of Aeronautics and Astronautics Basic Research Funded Project (Grant No. Y1065-063).

1 Wang T S, Zhang B G. The radio-voltaic effect applied to radioisotopic decay energy power generation. Nucl Tech, 1995, 18(012): 740–743
2 Zou Y, Huang N K. Basic principles and developments of the radioisotope powered voltaic batteries. Nucl Tech, 2006, 29(6): 432–437
3 Sun L, Yuan W Z, Qiao D Y. Research on a novel radioisotrope micro battery based on MEMS technology. J Funct Mater Devic, 2006, 12(005): 434–438
4 Guo H, Yang H, Zhang Y. Betavoltaic micro batteries using porous silicon. Proceedings of the 20th IEEE Micro Electro Mechanical Systems, Japan Kobe, 2007. 867–870
5 Deus S. Tritium-powered betavoltaic cells based on amorphous silicon. Conference Record of the Twenty-Eighth IEEE Photovoltaic Specialists Conference, 2000. 1246–1249
6 Qin C. Modeling and performance analysis of MEMS isotope microbattery. Xi'an: Northwestern Polytechnical University, 2007. 22–29
7 Guo H, Lal A. Nanopower betavoltaic microbatteries. Proceedings of 12th International Conference on Transducers, Solid-State Sensors, Actuators and Microsystems, 2003. 36–39
8 Xu S Y. Monte Carlo Methods in Experimental Nuclear Physics Applications. Beijing: Atomic Energy Press, 2006. 262–270
9 Briesmeister J F. MCNP-A general monte carlo n-particle transport code, Version 4C. LA-12625, 1993
10 Honsberg C. GaN betavoltaic energy converters. Conference Record of the Thirty-First IEEE Photovoltaic Specialists Conference, 2005. 102–105
11 Mohamadian S M, Feghhi S A H, Afarideh H. Analyze and simulation of a typical mems rpg using mcnp code. Icone16: Proceeding of the 16th International Conference on Nuclear Engineering, 2008, 1: 883–886
12 Anderson B L. Fundamentals of Semiconductor Devices. Boston: McGraw-Hill Higher Education, 2005. 83–120

© 1994-2012 China Academic Journal Electronic Publishing House. All rights reserved. http://www.cnki.net